Cross-machine comparison of resonant field amplification and resistive wall mode stabilization by plasma rotation[a)]

H. Reimerdes,[1,b)] T. C. Hender,[2] S. A. Sabbagh,[1] J. M. Bialek,[1] M. S. Chu,[3] A. M. Garofalo,[1] M. P. Gryaznevich,[2] D. F. Howell,[2] G. L. Jackson,[3] R. J. La Haye,[3] Y. Q. Liu,[4] J. E. Menard,[5] G. A. Navratil,[1] M. Okabayashi,[5] S. D. Pinches,[6] A. C. Sontag,[1] E. J. Strait,[3] W. Zhu,[1] M. Bigi,[2] M. de Baar,[7] P. de Vries,[2] D. A. Gates,[5] P. Gohil,[3] R. J. Groebner,[3] D. Mueller,[5] R. Raman,[8] J. T. Scoville,[3] W. M. Solomon,[5] the DIII-D Team, JET-EFDA Contributors,[c)] and the NSTX Team

[1]*Columbia University, New York, New York 10027*
[2]*EURATOM/UKAEA Fusion Association, Culham Science Centre, Abingdon, OX14 3DB, United Kingdom*
[3]*General Atomics, San Diego, California 92186–5608*
[4]*Chalmers University of Technology, S-412 96 Göteborg, Sweden*
[5]*Princeton Plasma Physics Laboratory, Princeton, New Jersey 08543–0451*
[6]*Max-Planck-Institut für Plasmaphysik, EURATOM Association, D-85748 Garching, Germany*
[7]*FOM Instituut for Plasmafysica Rijnhuizen, Association EURATOM-FOM, TEC, NL-343 BE Nieuwegein, The Netherlands*
[8]*University of Washington, Seattle, Washington 98195*

(Received 31 October 2005; accepted 26 January 2006; published online 11 May 2006)

Dedicated experiments in the DIII-D tokamak [J. L. Luxon, Nucl. Fusion, **42**, 614 (2002)], the Joint European Torus (JET) [P. H. Rebut, R. J. Bickerton, and B. E. Keen, Nucl. Fusion **25**, 1011 (1985)], and the National Spherical Torus Experiment (NSTX) [M. Ono, S. M. Kaye, Y.-K. M. Peng *et al.*, Nucl. Fusion **40**, 557 (2000)] reveal the commonalities of resistive wall mode (RWM) stabilization by sufficiently fast toroidal plasma rotation in devices of different size and aspect ratio. In each device the weakly damped $n=1$ RWM manifests itself by resonant field amplification (RFA) of externally applied $n=1$ magnetic fields, which increases with the plasma pressure. Probing DIII-D and JET plasmas with similar ideal magnetohydrodynamic (MHD) stability properties with externally applied magnetic $n=1$ fields, shows that the resulting RFA is independent of the machine size. In each device the drag resulting from RFA slows the toroidal plasma rotation and can lead to the onset of an unstable RWM. The critical plasma rotation required for stable operation in the plasma center decreases with increasing q_{95}, which is explained by the inward shift of q surfaces where the critical rotation remains constant. The quantitative agreement of the critical rotation normalized to the inverse Alfvén time at the $q=2$ surface in similar DIII-D and JET plasmas supports the independence of the RWM stabilization mechanism of machine size and indicates the importance of the $q=2$ surface. At low aspect ratio the required fraction of the Alfvén velocity increases significantly. The ratio of the critical rotation in similar NSTX and DIII-D plasmas can be explained by trapped particles not contributing to the RWM stabilization, which is consistent with stabilization mechanisms that are based on ion Landau damping. Alternatively, the ratio of the required rotation to the sound wave velocity remains independent of aspect ratio. © *2006 American Institute of Physics*. [DOI: 10.1063/1.2177134]

I. INTRODUCTION

The stabilization of the resistive wall mode (RWM) (Ref. 1) by rapid toroidal plasma rotation is a passive and, hence, attractive means to take advantage of wall stabilization in magnetic confinement devices. In the absence of plasma rotation the RWM becomes unstable when the normalized plasma pressure $\beta \equiv 2\mu_0 \langle p \rangle / B^2$ (where p is the plasma pressure, B is the toroidal magnetic field, and $\langle\ \rangle$ denotes volume averaging) exceeds the no wall limit $\beta_{\text{no wall}}$ set by a long-wavelength ideal magnetohydrodynamic (MHD) external kink mode in the absence of any conducting structure. The RWM has a similar structure as the external kink mode, but its growth is slowed by magnetic field penetration through conducting structures close to the plasma surface. RWM stabilization ultimately allows for an increase of β up to the ideal wall limit $\beta_{\text{ideal wall}}$ set by ideal MHD external kink modes, assuming that any nearby structures such as vacuum vessel or stabilizing plates were perfect conductors. Operation in this wall-stabilized regime is essential for steady-state advanced tokamak scenarios which rely on high plasma pressure for high fusion performance and high bootstrap current, but typically have broad current profiles with relatively low no wall limits and high ideal wall limits.[2–4] The stabilizing effect of toroidal plasma rotation in the order of a few percent of the Alfvén velocity on the RWM was first

[a)]Paper GI1 5, Bull. Am. Phys. Soc. **50**, 136 (2005).
[b)]Invited speaker. Electronic mail: reimerdes@fusion.gat.com
[c)]See J. Pamela *et al.*, Fusion Energy, in *Proceedings of the 20th International Conference*, Vilamoura, 2004 (IAEA, Vienna, 2004).

seen in the DIII-D tokamak[5] and has since been observed in the Joint European Torus (JET),[6] the High-Beta-Tokamak (HBT-EP),[7] and the National Spherical Torus Experiment (NSTX).[8] The ultimate potential of sustained operation at the ideal wall limit has been demonstrated in DIII-D discharges, effectively doubling the pressure above the no wall limit.[9] All observations of RWM stabilization by plasma rotation have been obtained in plasmas with predominant neutral beam injection (NBI) heating with a high momentum input. However, burning plasma experiments, such as ITER, have predominant α-particle heating and are expected to rotate much more slowly. It is important to know how much rotation will be necessary for reliable operation in the wall-stabilized regime.

The RWM interacts with plasma rotation since its growth rate and toroidal rotation frequency are limited to the order of the inverse of the characteristic field penetration time of the wall, τ_W, which is usually much slower than the toroidal plasma rotation, leading to a significant differential rotation between the plasma and the quasistatic magnetic perturbation. It has been shown numerically that plasma rotation in conjunction with a dissipative term in the ideal MHD equations can stabilize the RWM.[10] In the sound-wave damping model the perturbation of the plasma rotation caused by the RWM couples to sound waves, which are then subject to ion Landau damping. The sound wave damping is implemented by introducing a parallel viscous force in the ideal MHD equations. Subsequently, a more complete kinetic model of the interaction of plasma rotation with the perturbed field has been developed.[11]

The rotationally stabilized RWM is only weakly damped, which can make the plasma susceptible to nonaxisymmetric magnetic perturbation. Externally applied magnetic perturbation with a component that is resonant with the weakly damped RWM can excite a finite mode amplitude.[12] This process, which is referred to as resonant field amplification (RFA), has been used to explain the increased drag in DIII-D discharges with β above $\beta_{\text{no wall}}$.[13] RFA has subsequently been observed and studied in JET,[6,14] HBT-EP,[7] the EXTRAP T2R reversed-field pinch[15] and NSTX.[16,17] It is of operational concern, since the perturbed field exerts a torque on the plasma and can slow the plasma rotation, thereby nonlinearly destabilizing the RWM. If the externally applied field is well known, the RFA reveals the damping rate and mode rotation frequency of the stable RWM[18] and is used for active MHD spectroscopy.[19]

After individual observations of RWM stabilization by plasma rotation in the NSTX spherical torus and the DIII-D and JET tokamaks, a dedicated comparison is carried out in order to identify commonalities of RWM characteristics and to verify the physics models. The comparison includes the scaling of rotational stabilization with size between DIII-D and JET and with aspect ratio between DIII-D and NSTX. Some device parameters are listed in Table I. The three devices are equipped with sufficient heating power to exceed the no wall limit and have a wall that is close enough to open a substantial wall-stabilized regime. They are also equipped with nonaxisymmetric control coils, which are an essential tool to vary the plasma rotation independent of heating power by applying magnetic drag and to probe the RWM stability. For this comparison, plasmas with similar poloidal cross section shapes and safety factor profiles have been developed. The target plasmas are described in Sec. II. Quantitative comparisons are carried out by probing stable plasmas with externally applied resonant, $n=1$ magnetic fields in Sec. III, and by measuring the critical plasma rotation required for RWM stability, Ω_{crit} in Sec. IV. The results are summarized in Sec. V.

TABLE I. Machine parameters of the NSTX spherical torus and the DIII-D and JET tokamaks. The wall time τ_W is the characteristic decay time of a predominantly $m=1$ eddy current pattern.[6,20]

	NSTX	DIII-D	JET
Major radius R_0 (m)	0.86	1.69	2.96
Aspect ratio A	1.27	3.1	3.2
Wall time τ_W (ms)	5.0[a]	7.0	6.3

[a]In NSTX the wall time is given as a typical RWM growth time.

II. TARGET PLASMAS

The cross-machine comparison is carried out in two pairs with DIII-D matching the JET target[14] and with DIII-D and NSTX developing a common target shape. Both comparisons use a lower single-null shape. The targets are ELMy H-mode plasmas with broad current density profiles, to obtain good wall coupling of the kink mode and maximize the extent of the wall stabilized regime. The broadness of the current density profile is characterized by the internal inductance,

$$\ell_i \equiv \langle B_p^2 \rangle / \langle B_p \rangle^2, \tag{1}$$

where B_p is the poloidal field. Note that JET usually uses a different normalization of the internal inductance, which leads to different values. The minimum safety factor $q_{\min}$ is kept close to 1.5 with central shear being low or weakly reversed.

Since the goal of the comparison is to characterize the stabilizing effect of rotation on the RWM, a measure of the instability drive is needed. The normalized RWM growth $\gamma\tau_W$ depends on plasma parameters such as the pressure and current density profiles, which drive the RWM and the geometry of the resistive wall, which slows the growth of the mode. An approximate measure for the instability drive is the gain in β between the no wall and ideal wall stability limits set by the $n=1$ kink mode,[21]

$$C_\beta \equiv \frac{\beta - \beta_{\text{no wall}}}{\beta_{\text{ideal wall}} - \beta_{\text{no wall}}}. \tag{2}$$

In order to compare the toroidal plasma rotation Ω_{rot} in different devices, a characteristic time scale for the damping process has to be identified. The damping models[10,11] suggest the toroidal Alfvén time to be the relevant time scale. Here, the Alfvén time is defined as,

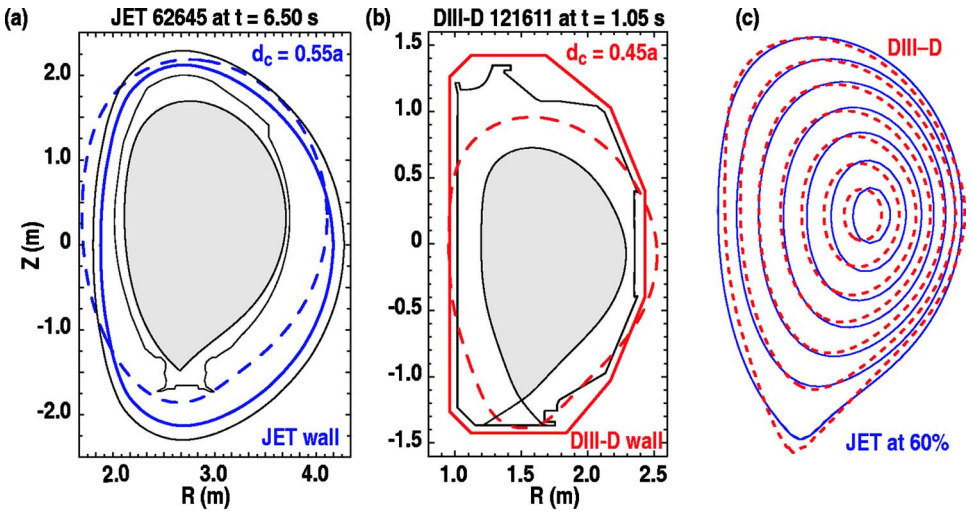

FIG. 1. (Color online) Geometry of the (a) JET and (b) DIII-D plasmas and wall components (tiles and vacuum vessel). The vessel component used as an ideal wall in the stability calculations is highlighted (solid) and the location of an effective conformal wall indicated (dashed). (c) Overlay of the scaled poloidal cross sections of the JET (solid) and DIII-D (dashed) plasmas.

$$\tau_A \equiv R_{\mathrm{mag}} \frac{\sqrt{\mu_0 n_e m_i}}{B_{\mathrm{mag}}}, \tag{3}$$

where R_{mag} and B_{mag} are the major radius and magnetic field on the magnetic axis, m_i the ion mass, and n_e the local electron density. Note that τ_A, according to Definition (3), is a flux surface quantity with the choice of B_{mag} and R_{mag} providing an element of flux surface averaging. The scaling of the critical rotation with τ_A^{-1} within a single device has been confirmed in DIII-D experiments.[22]

A. JET/DIII-D comparison

In the JET target plasma early heating during the plasma current ramp phase leads to a broad current density profile. The internal inductance ℓ_i ranges from 0.85 to 1.0. The use of up to 20 MW of NBI power and 4.7 MW of ion cyclotron resonance heating (ICRH) power at low toroidal field B_T, ranging from 0.8 to 1.4 T, resulted in values of β_N up to 3.7. Here $\beta_N \equiv \beta(\%)/\{I(\mathrm{MA})/[a(\mathrm{m})B(\mathrm{T})]\}$ is the customary normalization of β. In the experiments discussed here the safety factor q_{95} varied from 3.5 to 5.0. The poloidal plasma cross section is shown in Fig. 1(a) and typical plasma parameters are listed in Table II. Ideal MHD stability calculations using the MARS-F[23] and DCON[24] codes yield a no wall limit for the $n=1$ mode of $\beta_{N,\mathrm{no\ wall}} \approx 2.8\ell_i$. Note that this value of $\beta_{N,\mathrm{no\ wall}}/\ell_i$ is consistent with the value of 3.4 quoted in Ref. 14 since it uses a different definition of ℓ_i. The onset of the $m/n=2/1$ tearing mode at $\beta_N \approx 3.6$ is interpreted as the manifestation of the ideal wall limit,[25] which is consistent with DCON calculations. Thus, for a typical value of ℓ_i of 0.95, wall stabilization has the potential to increase β in these JET discharges 35% above the no wall limit.

A plasma with a JET-like shape has been developed in DIII-D, Fig. 1(b). The overlay of the shapes in Fig. 1(c) shows a good match. In these discharges early heating and a continued current ramp have been used to maintain a broad current density profile. The internal inductance ℓ_i is typically 0.7, which is significantly lower than in the JET experiment.

TABLE II. Typical plasma parameters in the cross-machine comparison experiment. The Alfvén time τ_A and sound time τ_S are defined in Eqs. (3) and (8), respectively.

	JET	DIII-D (JET shape)	NSTX	DIII-D (NSTX shape)
Toroidal field B_T (T)	0.8–1.4	1.8–2.1	0.44	2.1
Elongation κ	1.7	1.7	2.1	2.1
Upper/lower triangularity δ_u/δ_l	0.2/0.3	0.3/0.45	0.4/0.65	0.3/0.55
Internal inductance ℓ_i	~0.95	0.7	~0.7	~0.8
Ideal MHD no wall limit $\beta_{N,\mathrm{no\ wall}}$	~2.7 ($2.8\ell_i$)	~2.0 ($2.8\ell_i$)	4.0–4.8 (6–$7\ell_i$)	~1.9 ($2.4\ell_i$)
Ideal MHD ideal wall limit $\beta_{N,\mathrm{ideal\ wall}}$	~3.6	~3.0	⩾6	~3.0
Central ion temperature $T_{i,0}$ (keV)	~5.0	~5.6	~0.90	~9.2
Central electron temperature $T_{e,0}$ (keV)	~4.0	3.1	~0.84	~3.6
Central electron density $n_{e,0}$ ($10^{19}/\mathrm{m}^3$)	~2.7	~6.3	~7.0	~5.1
Alfvén time $\tau_{A,0}$ (μs)	~0.9	0.5	1.6	0.4
Sound time $\tau_{S,0}$ (μs)	~4.8	2.8	~3.8	~2.3

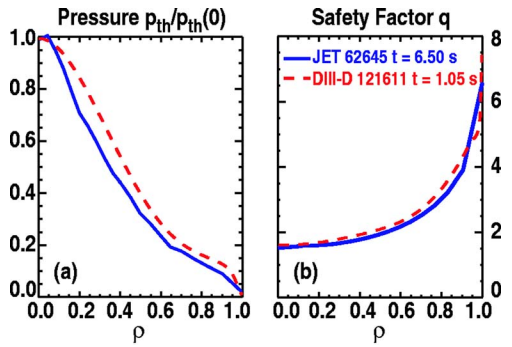

FIG. 2. (Color online) (a) Thermal pressure p_{th} and (b) safety factor q profiles in the JET (solid) and corresponding DIII-D (dashed) experiments.

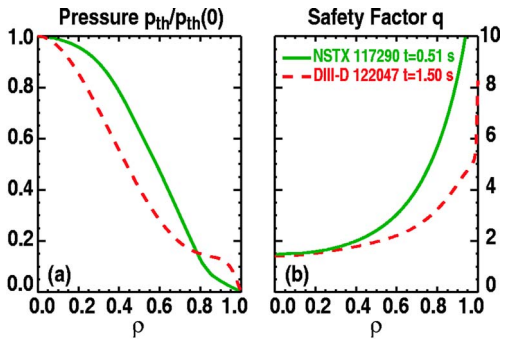

FIG. 4. (Color online) (a) Thermal pressure p_{th} and (b) safety factor q profiles in the NSTX (solid) and corresponding DIII-D (dashed) experiment.

In the experiments discussed here, q_{95} varied from 4.0 to 4.6. The pressure and safety factor profiles are similar to the profiles obtained in JET, Fig. 2. Stability calculations with MARS-F and DCON yield a no wall stability limit of $\beta_{N,\mathrm{no\ wall}} \approx 2.8\ell_i$. Thus, the match of plasma shape and profiles in both devices results in the same ideal MHD no wall stability limit, within its dependence on ℓ_i. DCON indicates an ideal wall limit at $\beta_{N,\mathrm{ideal\ wall}} \approx 3.0$. As in the JET the approach of the ideal wall limit in DIII-D also results in the onset of 2/1 tearing modes. For a typical value of $\ell_i \approx 0.7$, wall stabilization can increase β up to 50% above the no wall limit in these DIII-D plasmas.

The wall position is an important parameter for RWM stability. Since the wall geometry varies greatly among the devices, the position of an effective conformal wall is determined. The effective conformal wall is placed at a distance d_c from the plasma surface so that ideal wall stability limit calculations using DCON yield the same value of $\beta_{N,\mathrm{ideal\ wall}}$ as the actual wall in the experiment. This results in an effective conformal wall for the JET experiment at a distance of $d_c = 0.55a$, Fig. 1(a), compared to $d_c = 0.45a$ in the DIII-D experiment in the JET shape, Fig. 1(b). A closer effective conformal wall and the broader current profile in these DIII-D plasmas are responsible for the larger extent of the wall-stabilized regime in DIII-D compared to JET.

The Alfvén time in the center of DIII-D discharges in this experiment is typically $\tau_{A,0} \approx 0.5\ \mu$s, while the values in JET of $\tau_{A,0} \approx 0.9\ \mu$s are typically higher.

B. NSTX/DIII-D comparison

The target plasma shape for the NSTX/DIII-D comparison has an elongation of $\kappa = 2.1$. In the NSTX part of the experiment up to 6.6 MW of NBI power are injected into the target plasma with a toroidal field of $B_T = 0.44$ T, resulting in values of β_N up to 6, Fig. 3(a). The internal inductance ℓ_i ranges from 0.65 to 0.75. The safety factor q_{95} is varied from 8 to 10. Figure 4 shows the pressure and safety factor profiles and Table II lists typical discharge parameters. The no wall stability limit is calculated with DCON and ranges from $\beta_{N,\mathrm{no\ wall}} = 6-7\ell_i$. Variations in pressure peaking have a stronger influence on the value of $\beta_{N,\mathrm{no\ wall}}$ than ℓ_i.[8] Experimental access to values of $\beta_N \approx 6$ indicates $\beta_{N,\mathrm{ideal\ wall}} \geqslant 6$.

The corresponding DIII-D plasma is shown in Fig. 3(b). While the plasma boundaries are reasonably well matched with DIII-D having a slightly lower elongation κ and triangularity δ, internal flux surfaces deviate more, Fig. 3(c). The

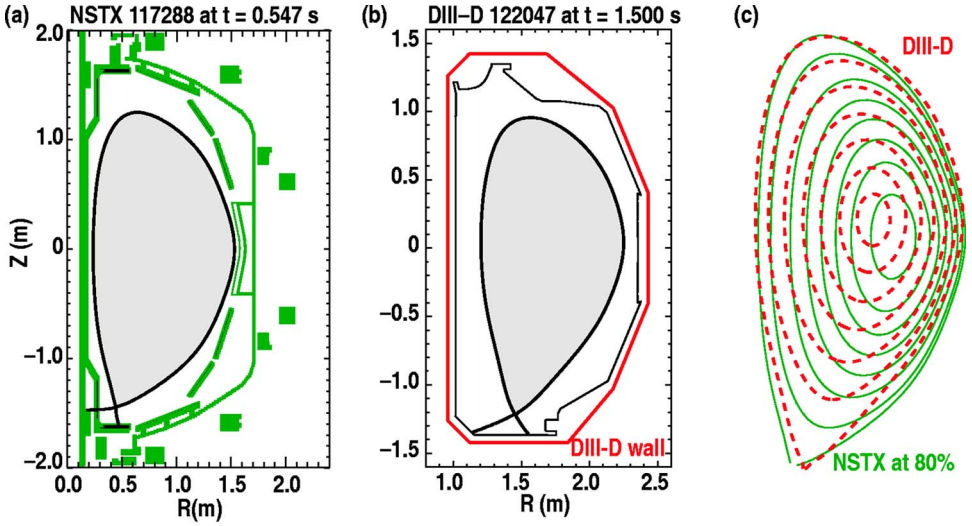

FIG. 3. (Color online) Geometry of the (a) NSTX and (b) DIII-D plasmas and wall components. (c) Overlay of the scaled poloidal cross sections of the NSTX (solid) and DIII-D (dashed) plasmas.

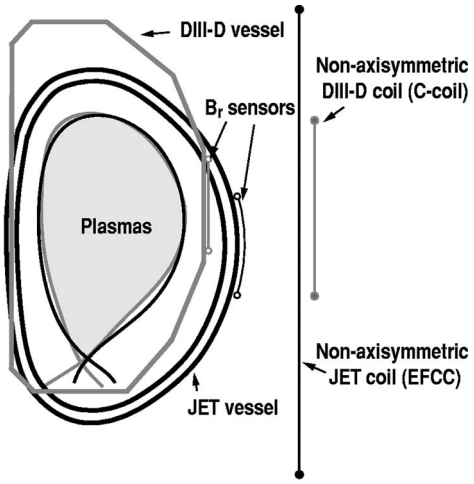

FIG. 5. Comparison of the geometry of nonaxisymmetric coils and sensor arrays with respect to the plasma in JET (black) and DIII-D (gray). The size of the JET plasma, wall and coils are reduced by 60%.

difficulty to match plasmas at different aspect ratios is also seen in the pressure and safety factor profiles shown in Fig. 4. In the DIII-D part of the experiment ℓ_i ranges from 0.75 to 0.85 and q_{95} from 4.2 to 5.4, which is significantly lower than in its low aspect ratio counterpart. Calculations with DCON yield a no wall stability of $\beta_{N,\text{no wall}} \approx 2.4\ell_i$ and an ideal wall limit of $\beta_{N,\text{ideal wall}} \approx 3.0$. For a typical value of $\ell_i = 0.8$, wall stabilization can increase β by 55%.

The Alfvén time in the center of DIII-D discharges in this experiment is typically $\tau_{A,0} \approx 0.4$ μs, while the values in NSTX of $\tau_{A,0} \approx 1.6$ μs are significantly higher.

III. RESONANT FIELD AMPLIFICATION

The no wall stability limit is generally set by the $n=1$ mode. Similarly, the observed RFA in the wall-stabilized regime is related to the rotationally stabilized $n=1$ mode. Higher n modes can become important at higher values of β. Resonant field amplification is usually measured as the ratio of the plasma response B_s^{plas} and the externally applied field B_s^{ext},

$$A_{\text{RFA},s} \equiv \frac{B_s^{\text{plas}}}{B_s^{\text{ext}}}. \tag{4}$$

Here, a complex notation is used to account for the toroidal phase of the $n=1$ component of the magnetic fields B_s^{plas} and B_s^{ext}.[19] The index s denotes the sensor array. Note that the RFA amplitude according to Definition (4) depends strongly on the location of the sensors, the measured field component, the geometry of applied field, and the mode structure of the plasma response.

A. Machine size comparison (DIII-D/JET)

The RFA in DIII-D and JET is compared by probing the target plasma with pulsed magnetic fields using a pair of external nonaxisymmetric control coils. The C-coil in DIII-D and the error field correction coil (EFCC) in JET have a similar geometry, Fig. 5, and both apply a field with a dominant $n=1$ component. The perturbation is measured with radial field probes located close to the vacuum vessels, also shown in Fig. 5. The perturbation amplitude has to be small in order to limit the perturbation of the target plasma, notably β and Ω_{rot}, to a minimum, Fig. 6. The pulses are long with respect to characteristic eddy current decay times, τ_W and result in a static plasma response. The plasma response is clearly seen at the node of the applied field, where the entire measured signal originates from the plasma response, Figs. 6(d) and 6(h). Note that a plasma response at the node of the applied field implies a toroidal phase shift between B_s^{plas} and B_s^{ext}.

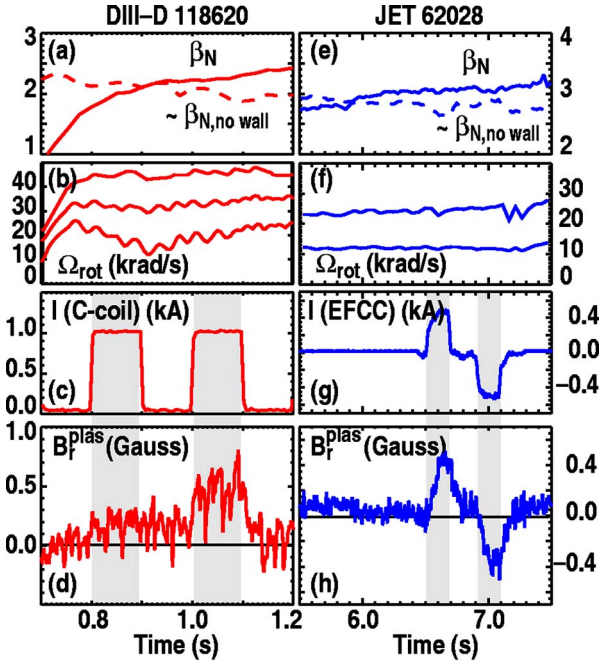

FIG. 6. (Color online) DIII-D and JET target plasmas, in which β_N exceeds the estimated $\beta_{N,\text{no wall}}$ (a,e), plasma rotation (b,f) stabilizes the RWM. The targets are probed with externally applied nonaxisymmetric fields (c,g). At high β a plasma response is observed as a perturbation of the radial field B_r at the node of the applied field (d,h).

1. β-dependence of RFA

In both devices the RFA is seen to increase significantly once β is close to or above $\beta_{\text{no wall}}$. The β dependence of the ratios of the plasma response at the node and the applied field at the toroidal location of the coil for DIII-D and JET are shown in Figs. 7(a) and 7(b), respectively. This ratio corresponds to the imaginary part of $A_{\text{RFA},s}$, Definition (4). A positive ratio indicates the characteristic phase shift of the plasma response in the direction of plasma rotation.[13] In DIII-D the amplification measurements at values of β below $\beta_{\text{no wall}}$ are below the noise level of the magnetic measurements and fluctuate around zero. Once β exceeds $\beta_{\text{no wall}}$ the RFA rapidly increases up to values of 0.1, as shown in Fig. 7(a). In JET the RFA measurements at the node of the applied field also increase significantly with β once it exceeds $\beta_{\text{no wall}}$ from values of 0.02 up to 0.04 as shown in Fig. 7(b). Contrary to the DIII-D observations JET shows a low but systematically positive plasma response even at the lowest values of β. Such a low β response has already been ob-

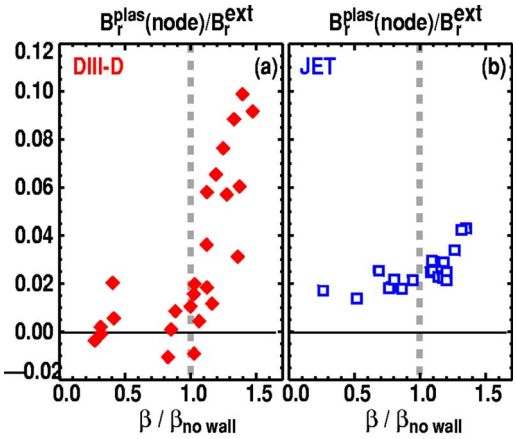

FIG. 7. (Color online) β dependence of the RFA in (a) DIII-D and (b) JET measured at the node of the applied $n=1$ field using B_r sensors at the vacuum vessel wall. This corresponds to the imaginary part of $A_{\mathrm{RFA},s}$ defined in Eq. (4).

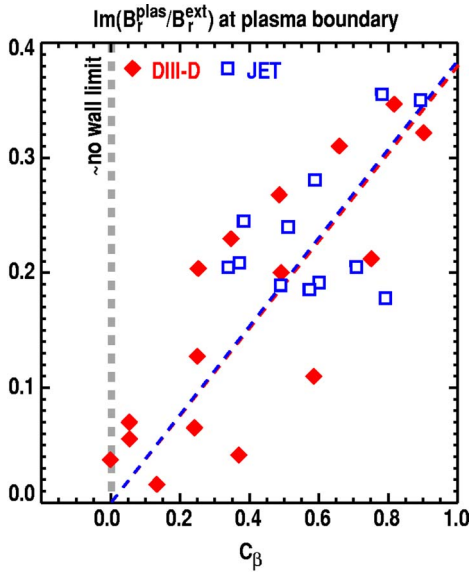

FIG. 9. (Color online) β dependence of the RFA measured at the node of the applied $n=1$ field and extrapolated to the plasma boundary in DIII-D (diamonds) and JET (squares). Each data set is fitted to a line through 0 (dashed).

served in previous JET experiment using internal nonaxisymmetric coils.[14] In the wall-stabilized regime the β dependence of RFA in JET has the same characteristics as in DIII-D, but the absolute value of the amplification is less than half.

The observed β dependence of the RFA at high β in these DIII-D and JET experiments is in qualitative agreement with RFA measurements in previous DIII-D[18] and NSTX[16,17] experiments, where high-β plasmas were probed with externally applied nonaxisymmetric fields with large $n=1$ components. In both experiments the RFA magnitude was seen to increase with β.

2. Comparison of RFA in different devices

The RFA measurement strongly depends on the geometry of the applied field, on the geometry of the plasma response and on the location of the magnetic sensors. The geometry of the applied fields in DIII-D and JET is similar, but the different radial positions of the magnetic sensors have to be accounted for by extrapolating the externally applied field and the plasma response to the same radial position, such as the plasma boundary. A schematic of the radial dependence of B^{plas} and B^{ext} in cylindrical geometry is shown in Fig. 8. While the externally applied field decreases from the sensor to the plasma, the plasma response decreases from the plasma to the sensor. In a cylindrical approximation the ratio of the RFA at the plasma boundary and the RFA measured with a sensor s is,

$$\frac{B_a^{\mathrm{plas}}/B_a^{\mathrm{ext}}}{B_s^{\mathrm{plas}}/B_s^{\mathrm{ext}}} = \left(\frac{r_s}{a}\right)^{2m}, \tag{5}$$

where r_s is the radial position of the sensor and m is the poloidal mode number. Assuming an effective poloidal mode number at the outboard midplane of $m=2$, the RFA at the DIII-D plasma boundary is 3.5 times larger than at the DIII-D sensors whereas the RFA at the JET boundary is 8.25 times larger than at the JET sensors. Evaluating the RFA at the plasma boundary in plasmas at the same RWM instability drive C_β, results in surprisingly good agreement between DIII-D and JET, Fig. 9. The simplified treatment of the geometry, in particular the choice of m and the unknown source of the low β plasma response in JET introduce a significant uncertainty in the quantitative comparison.

In a single mode model, the RFA is directly related to the growth rate γ_{RWM} and rotation frequency ω_{RWM} of the stable RWM,[18] The imaginary part of $A_{\mathrm{RFA},s}$, Definition (4), measured in these experiments, is determined by,[19]

$$\Im(A_{\mathrm{RFA},s}) \propto \frac{\omega_{\mathrm{RWM}}}{(\gamma_{\mathrm{RWM}}^2 + \omega_{\mathrm{RWM}}^2)\tau_W^*}. \tag{6}$$

Here, the wall time τ_W^* refers to the characteristic decay time of eddy current patterns induced by a RWM, which are generally dominated by $m \gg 1$ mode components, leading to somewhat smaller values than quoted for τ_W in Table I. The quantitative agreement of the measured values of $\Im(A_{\mathrm{RFA},s})$ in DIII-D and JET indicates similar RWM damping rates and mode rotation frequencies in both devices.

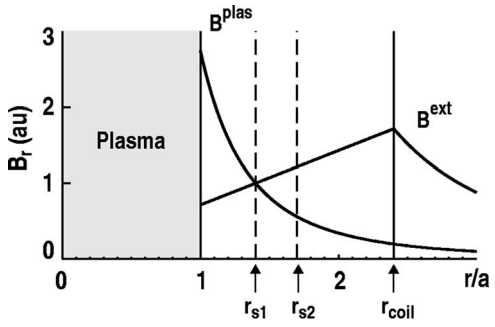

FIG. 8. Schematic of the dependence of the measurement of RFA $=B_s^{\mathrm{plas}}/B_s^{\mathrm{ext}}$ on the radial location r_{s1} and r_{s2} of different sensors arrays.

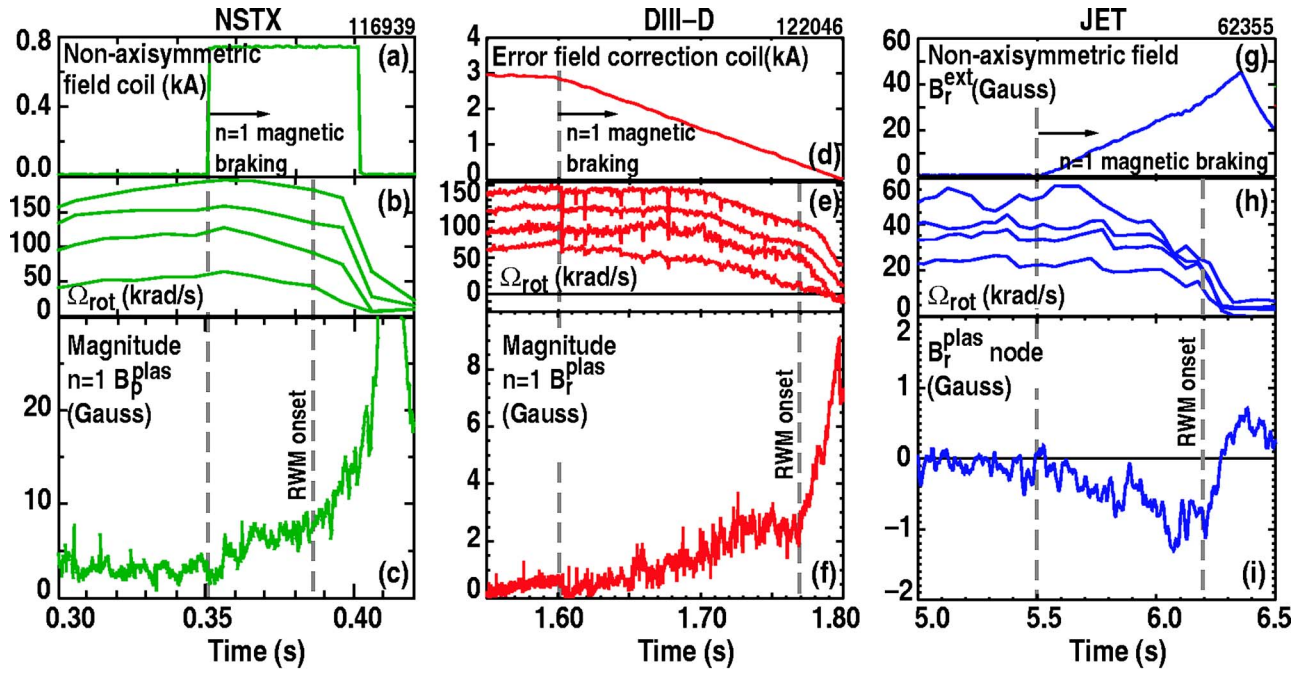

FIG. 10. (Color online) RWM onset in NSTX (a–c), DIII-D (d–f) and JET (g–i) discharges where $n=1$ magnetic fields were applied (a,d,g) to decelerate the plasma rotation Ω_{rot} (b,e,h) below Ω_{crit}. The evolution of the $n=1$ plasma response B^{plas} shows the onset of the unstable RWM (c,f,i).

IV. CRITICAL PLASMA ROTATION FOR RWM STABILIZATION

Ultimately, one wants to know how much rotation is required for reliable operation in the wall-stabilized regime. The plasma rotation at marginal stability is referred to as the critical rotation Ω_{crit}. Motivated by predictions that the dissipation occurs in the vicinity of resonant surfaces,[26] previous work has focused on the rotation at the $q=2$ surface.[14,22,27] It is, however, possible that the critical rotation depends on several resonant surfaces or the entire rotation profile.[16]

The plasma rotation is measured with charge exchange recombination (CER) spectroscopy using C^{6+}. It has recently been recognized that the energy dependence of the charge exchange cross section leads to a relatively important correction of rotation measurements in plasmas which have high ion temperatures, but low rotation.[28] This correction is particularly important in DIII-D and can lead to a significant correction of previously reported results.[29]

A. RWM onset

In the three devices investigated, the wall stabilized regime can only be accessed using NBI heating with a significant net torque, which generally leads to sufficiently fast plasma rotation for RWM stabilization. In order to observe the unstable RWM, the rotation is reduced by applying a static, nonaxisymmetric magnetic field. The magnetic field can be resonant ($n=1$) with the weakly damped RWM or nonresonant ($n \gg 1$). Note that *resonant* refers to the global kink mode and not a single flux surface. In the case of resonant braking, the resulting RFA also leads to an enhanced drag.[12,13,30] A resonant component from uncorrected intrinsic error fields is almost unavoidable. In the case of resonant braking a growing perturbed field is observed even before the RWM is unstable. At marginal stability ($\gamma_{RWM}=0$), the single mode model predicts a linear growth of the perturbation.[31] Since the RFA changes the plasma rotation and hence, the growth rate of the mode on a time scale comparable to the wall time τ_W, the evolution of the perturbed field is expected to be faster than linear. A nonzero mode rotation frequency ω_{RWM} can further complicate the evolution of the perturbed field at the RWM onset.

In these experiments the decrease of the rotation is accompanied with increased RFA. At some point in time both the slowing of plasma rotation and the perturbed field growth accelerate significantly. This time t_{onset} is used for the measurement of Ω_{crit}. The fast growth of the perturbation is interpreted as the RWM growth without the stabilizing effect of plasma rotation. It is, therefore, possible that t_{onset} determined in such a way is systematically late. The resulting uncertainty of Ω_{crit} should, however, be small since the plasma rotation prior to t_{onset} changes on a slow time scale.

In NSTX the RWM can grow spontaneously, without magnetic braking.[8] In this experiment magnetic braking is used to control the time of the RWM onset, Fig. 10(a). The applied $n=1$ field causes a deceleration of the plasma, Fig. 10(b). Resonant field amplification leads to a plasma response B^{plas} even before the RWM becomes unstable, Fig. 10(c). The onset of an accelerated growth of B^{plas} marks t_{onset}.

In DIII-D a reduction of nonaxisymmetric coil currents correcting the intrinsic error field is sufficient to slow down the plasma rotation, Figs. 10(d) and 10(e). The evolution of the $n=1$ plasma response in DIII-D, Fig. 10(f), is similar to the observations in NSTX, Fig. 10(c), showing increasing

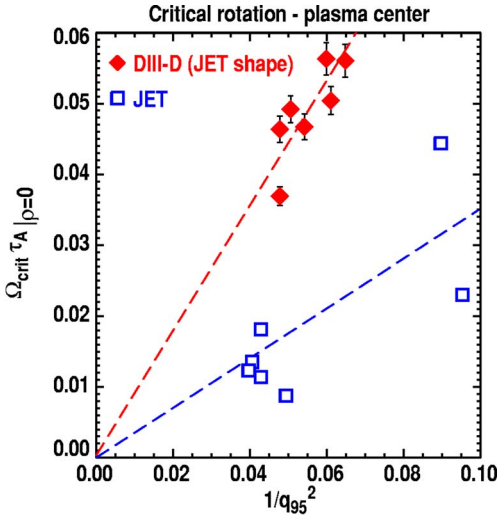

FIG. 11. (Color online) Central normalized critical rotation in DIII-D (diamonds) and JET (squares) indicate a $1/q_{95}^2$ dependence in each device.

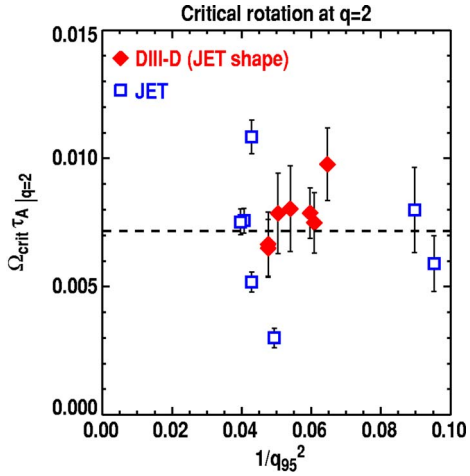

FIG. 12. (Color online) Evaluating the normalized critical rotation at the $q=2$ surface removes the q_{95} dependence and leads to quantitative agreement in DIII-D (diamonds) and JET (squares).

RFA prior to the RWM onset. The RWM onset usually leads to a fast rotation collapse. The RWM grows on time scales ranging from 2 to 20 ms.

In JET the plasma rotation can be reduced by replacing NBI heating power with ion cyclotron resonance heating power. However, in order to obtain sufficiently low plasma rotation for a RWM onset, a magnetic field with a dominant $n=1$ structure is applied with the nonaxisymmetric field coil (EFCC), Figs. 10(g) and 10(h). RFA followed by a RWM onset is clearly observed at the node of the applied field, Fig. 10(i). The RWM typically grows on time scales ranging from 50 to 100 ms. Note that these growth times are surprisingly slow compared to the characteristic time of the JET wall, Table I and remains to be understood.

B. Machine size comparison (DIII-D/JET)

The main difference between the DIII-D and the JET plasmas is the dimensions of the plasma and machine. Since the instability drive depends on matched parameters such as shape, q profile and C_β, it is expected that the same plasma rotation normalized with the Alfvén velocity is required for stability.

1. q_{95}-dependence

Since previous experiments[14,27] have suggested a dependence of Ω_{crit} on q_{95}, the cross-machine comparison is carried out at various values of q_{95}. It is found that the central plasma rotation at marginal stability, normalized with the inverse Alfvén time, in DIII-D and JET increases with decreasing q_{95}. The measurements in both devices support a $|\Omega_{crit}\tau_A|_{\rho=0} \propto 1/q_{95}^2$ dependence, Fig. 11, albeit with different proportionality factors. The critical rotation in the center of JET plasma is distinctly lower than in DIII-D. The observed q_{95} dependence is in good agreement with predictions for the kinetic damping model using the MARS-F code.[32]

Increasing q_{95} leads to an increase of the safety factor at each location in the plasma. The observed q_{95} dependence could, therefore, be caused by an increasing stabilizing effect of plasma rotation as q increases. This is consistent with the prediction of toroidal inertia enhancement for the kinetic damping model, leading to a $\Omega_{crit} \propto 1/q^2$ dependence.[11] The increase of the local safety factor also implies that rational surfaces move inwards, towards higher plasma rotation. Evaluating the normalized critical rotation at the $q=2$ surface removes not just the q_{95} dependence, but also the difference between the two devices as shown in Fig. 12. This supports the predictions for the sound wave damping model[26] that the stabilization predominantly takes place at the $q=2$ surface. Note that due to the magnetic braking the rotation at higher integer surfaces is close to zero and, therefore, does not contribute to the stabilization. It can, however, not be ruled out that the Ω_{rot} profile in DIII-D, which is more peaked than the profile in JET, provides more stabilization inside the $q=2$ surface, which is compensated for by less rotation outside $q=2$. Variations of rotation profile shape are also a potential source for the variations of the $|\Omega_{crit}\tau_A|_{q=2}$ measurements in Fig. 12.

2. β-dependence

Some variations of the $|\Omega_{crit}\tau_A|_{q=2}$ measurements can be explained by variations in the value of β. While the DIII-D measurements are taken at similar values of β the JET values span the entire wall-stabilized regime. Figure 13 shows the β dependence, indicating the reduction of Ω_{crit} in the vicinity of the no wall limit $C_\beta=0$. Note that the data points at values of C_β below 0 and above 1 arise from the uncertainties of the values for $\beta_{no\ wall}$ and $\beta_{ideal\ wall}$, which are used to determine C_β, Table II. In particular, they neither indicate a RWM onset below $\beta_{no\ wall}$ nor operation above $\beta_{ideal\ wall}$. The decrease of the Ω_{crit} close to the no wall limit suggests that at constant rotation the RWM damping increases. This is consistent with the observed β dependence of the RFA close to the no wall limit, shown in Sec. III A 1.

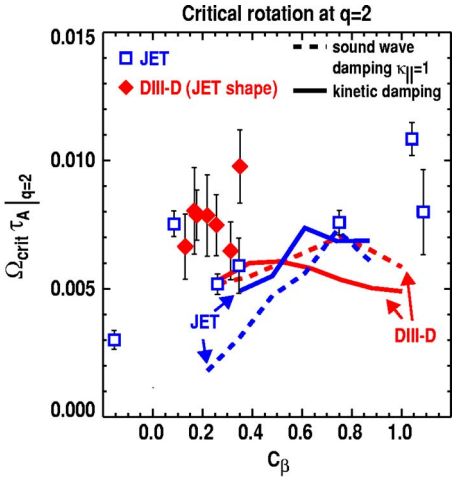

FIG. 13. (Color online) Measurements of the normalized critical rotation at the $q=2$ surface in DIII-D (diamonds) and JET (squares) as a function of C_β show a weak β dependence. The C_β values <0 and >1 are a reflection of the uncertainties of the calculated β limits. The critical rotation is predicted by the sound wave (dashed) and kinetic damping model (solid).

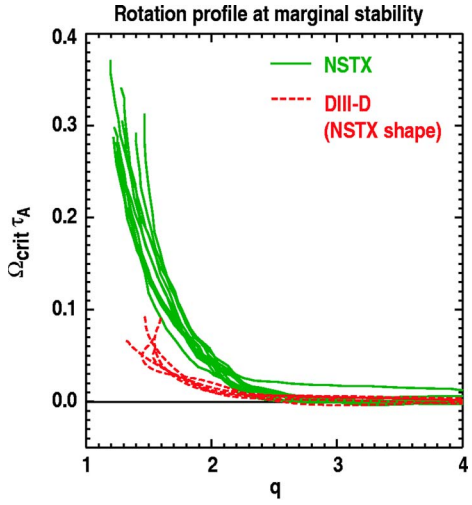

FIG. 14. (Color online) Normalized plasma rotation at marginal stability $\Omega_{crit}\tau_A$ in NSTX (solid) and DIII-D (dashed) as a function of the safety factor q.

3. Comparison with modeling

The measured critical rotation is compared to predictions for the sound wave damping and the kinetic damping model using the MARS-F code.[23] In the sound wave damping model the parameter $\kappa_{||}$ is set to 1. The calculations are carried out for a DIII-D and a JET equilibrium of this experiment. The experimental pressure is scaled to span a large fraction of the wall stabilized regime. For $C_\beta > 0.4$ both damping models predict a similar critical rotation for both experiments ranging from $|\Omega_{crit}\tau_A|_{q=2}=0.004$ to 0.007, Fig. 13. In particular the kinetic damping model shows only a weak β dependence and typically underestimates the measurements by less than 30%. Considering the significant uncertainties of the measurements, the comparison of the model predictions with the experiment is promising.

C. Aspect ratio comparison (DIII-D/NSTX)

In the DIII-D and NSTX comparison, the shape of the poloidal plasma cross section is well matched. Due to the good match of the RFA and critical rotation in JET and DIII-D, differences between DIII-D and NSTX can be mainly attributed to the aspect ratio, which varies by a factor of 2.

The change of the critical rotation in NSTX with q_{95} is in qualitative agreement with the DIII-D and JET observations. In particular, evaluating Ω_{crit} at the same value of q removes the q_{95} dependence. In both devices, DIII-D and NSTX, the magnetic braking leads to peaked rotation profiles at marginal stability, with Ω_{rot} for $q \geq 3$ being close to zero. This observation demonstrates that a single resonant surface can be sufficient for RWM stabilization. A comparison of the rotation profiles at marginal stability of several DIII-D and NSTX discharges, shown as a function of q in Fig. 14, reveals that the critical rotation in NSTX exceeds the critical rotation in DIII-D at each value of q (where the rotation is larger than zero).

Comparing the measurements at the $q=2$ surface in NSTX and DIII-D illustrates the aspect ratio dependence, Fig. 15. The measurements in each device show significant variations. In DIII-D, C_β ranges from 0.2 to 0.5. Note that $|\Omega_{crit}\tau_A|_{q=2}$ in DIII-D plasmas in the NSTX shape is significantly higher than in the JET shape. While β_N in NSTX varies from 4.3 to 5.2, the variations of $|\Omega_{crit}\tau_A|_{q=2}$ are not correlated with variations of β_N. It is possible that changes of the pressure peaking and, hence, of β limits, mask a C_β dependence. Despite the variation in the measurements, $|\Omega_{crit}\tau_A|_{q=2}$ clearly increases with increasing inverse aspect ratio ϵ. The decrease of rotational stabilization with increasing ϵ can be explained by a strongly reduced contribution of trapped particles to the RWM stabilization expected for ion Landau damping. If trapped particles do not contribute at all, the critical rotation is expected to be inversely proportional to the fraction of passing particles

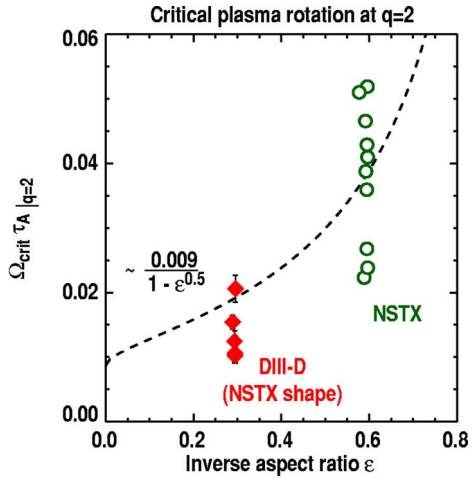

FIG. 15. (Color online) The normalized critical rotation at the $q=2$ surface in DIII-D (squares) and NSTX (circles) increases with the inverse aspect ratio ϵ. The measurements are fitted to a $1/(1-\sqrt{\epsilon})$ dependence.

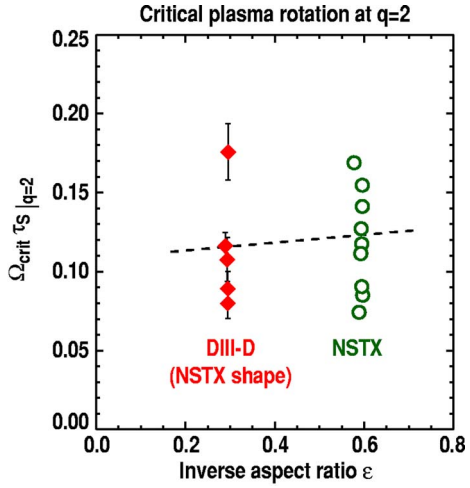

FIG. 16. (Color online) The normalization of the critical rotation at the $q=2$ surface with the inverse of the sound time τ_S tends to remove the aspect ratio dependence seen between DIII-D (squares) and NSTX (circles). A linear fit (dashed) results in an almost horizontal line.

$$\Omega_{\text{crit}} \propto \frac{1}{1-\sqrt{\epsilon}}. \tag{7}$$

According to Eq. (7) an increase of ϵ from 0.3 (DIII-D) to 0.6 (NSTX) should result in a doubling of Ω_{crit} consistent with the observations in DIII-D and NSTX, Fig. 15. Contrary to the sound wave damping model, the kinetic damping model treats trapped and passing particles differently and should, therefore, be able to correctly describe the aspect ratio dependence of RWM stabilization by plasma rotation.

The comparison of plasmas at different aspect ratios allows for a decoupling of the Alfvén time τ_A from the sound wave time τ_S defined as,

$$\tau_S \equiv R_{\text{mag}} \sqrt{\frac{m_i}{k_B T_e + k_B T_i}}, \tag{8}$$

where T_e and T_i are the electron and ion temperatures at a flux surface. The two time scales are coupled via ϵ, β_N, and q_{95} with $\tau_A/\tau_S \propto (\epsilon\beta_N/q_{95})^{1/2}$. [22] While the ratio of τ_A and τ_S is the same in DIII-D and JET, it changes with the aspect ratio. Normalizing the Ω_{crit} measurements at the $q=2$ surface in NSTX and DIII-D with the inverse of the sound time removes the aspect ratio dependence almost entirely, Fig. 16.

V. SUMMARY

Dedicated experiments in the DIII-D and JET tokamaks and the NSTX spherical torus show the universal characteristics of RWM stabilization by plasma rotation. In each of the three devices the weakly damped $n=1$ mode manifests itself in RFA above the no wall stability limit. Despite the difference in size of the DIII-D and JET plasmas, the RFA resulting from externally applied $n=1$ fields with similar geometry is in quantitative agreement, when taking into account geometrical corrections. The RWM becomes unstable once the plasma rotation decreases below a critical value. While the observed RWM growth rates in DIII-D and NSTX are in the order of the inverse of the characteristic wall times, the significantly slower RWM growth in JET remains to be understood.

The critical rotation in the plasma center is seen to increase with decreasing q_{95}, which is consistent with the $1/q_{95}^2$ dependence suggested by predictions of the kinetic damping model using the MARS-F code.[32] This q_{95} dependence is explained by q surfaces moving inwards toward higher plasma rotation. In the experiments presented here, the $q=2$ surface is of particular importance. Evaluating Ω_{crit} at the $q=2$ surface results in quantitative agreement between DIII-D and JET. Since the magnetic braking leads to very low or zero rotation at higher integer q surfaces, it cannot be excluded that these surfaces contribute to RWM stabilization in unperturbed rotation profiles. The comparison between Ω_{crit} in DIII-D and NSTX reveals a significantly higher critical rotation at low aspect ratio, when it is normalized with the inverse Alfvén time. The ratio of $\Omega_{\text{crit}}\tau_A$ at the $q=2$ surface is in good agreement with a model, where trapped particles do not contribute to the RWM stabilization. It is, therefore, expected that the kinetic damping model will correctly describe the observed aspect ratio dependence. Alternatively, normalizing Ω_{crit} with the inverse sound time removes the aspect ratio dependence.

The comparison of the critical rotation in the DIII-D and JET experiments with predictions by the sound wave damping model using $\kappa_{\|}=1$ and the kinetic damping model yields promising results. The kinetic model, in particular, underestimates the critical rotation by less than 30%. The observations in the aspect ratio comparison provide a new opportunity to test the damping models.

ACKNOWLEDGMENTS

H. Reimerdes would like to thank D. Bulmer, T.A. Casper, W.M. Meyer, and D. Pearlstein for their help and support with the CORSICA package.

This work was supported by the U.S. Department of Energy under Contract Nos. DE-FG02-89ER543297, DE-FG03-95ER54309, DE-FC02-04ER54698, DE-AC02-76CH03073, and partly conducted under the European Fusion Development Agreement.

[1] J. P. Freidberg, *Ideal Magnetohydrodynamics* (Plenum, New York, 1987).
[2] C. Kessel, J. Manickam, G. Rewoldt, W. M. Tang, Phys. Rev. Lett. **72**, 1212 (1994).
[3] A. D. Turnbull, T. S. Taylor, Y. R. Lin-Liu, and H. St. John, Phys. Rev. Lett. **74**, 718 (1995).
[4] T. S. Taylor, E. J. Strait, L. L. Lao *et al.*, Phys. Plasmas **2**, 2390 (1995).
[5] E. J. Strait, T. S. Taylor, A. D. Turnbull, J. R. Ferron, L. L. Lao, B. Rice, O. Sauter, S. J. Thompson, and D. Wróblewski, Phys. Rev. Lett. **74**, 2483 (1995).
[6] M. P. Gryaznevich, C. G. Gimblett, T. C. Hender, D. F. Howell, S. Pinches, R. J. La Haye, Y. Q. Liu, and A. Bondeson, Bull. Am. Phys. Soc. **48**, 307 (2003).
[7] M. Shilov, C. Cates, R. James *et al.*, Phys. Plasmas **11**, 2573 (2004).
[8] S. A. Sabbagh, J. M. Bialek, R. E. Bell *et al.*, Nucl. Fusion **44**, 560 (2004).
[9] A. M. Garofalo, E. J. Strait, L. C. Johnson *et al.*, Phys. Rev. Lett. **89**, 235001 (2002).
[10] A. Bondeson and D. J. Ward, Phys. Rev. Lett. **72**, 2709 (1994).
[11] A. Bondeson and M. S. Chu, Phys. Plasmas **3**, 3013 (1996).
[12] A. H. Boozer, Phys. Rev. Lett. **86**, 1176 (2001).
[13] A. M. Garofalo, T. H. Jensen, L. C. Johnson *et al.*, Phys. Plasmas **9**, 1997

(2002).
[14]T. C. Hender, M. Gryaznevich, Y. Q. Liu *et al.*, in *20th IAEA Fusion Energy Conference 2004*, Vilamoura, Portugal, 1–6 November 2004 (IAEA, Vienna, 2004), paper No. EX/P2-22.
[15]J. R. Drake, P. R. Brunsell, D. Yadikin *et al.*, Nucl. Fusion **45**, 557 (2005).
[16]A. C. Sontag, S. A. Sabbagh, W. Zhu *et al.*, Phys. Plasmas **12**, 056112 (2005).
[17]S. A. Sabbagh, A. C. Sontag, J. M. Bialek *et al.*, in *20th IAEA Fusion Energy Conference 2004*, Vilamoura, Portugal, 1–6 November 2004 (IAEA, Vienna, 2004), EX/3-2.
[18]A. M. Garofalo, T. H. Jensen, and E. J. Strait, Phys. Plasmas **10**, 4776 (2003).
[19]H. Reimerdes, M. S. Chu, A. M. Garofalo *et al.*, Phys. Rev. Lett. **93**, 135002 (2004).
[20]J. T. Scoville, D. H. Kellman, A. Nerem, S. G. E. Pronko, D. ONeill, G. Rossi, R. Hatcher, and M. Bolha, in *Proceedings of the 18th IEEE/NPSS Symposium on Fusion Engineering*, Albuquerque, New Mexico, October 25–29, 1999 (Institute of Electrical and Electronics Engineers, Piscataway, NJ, 1999), p. 198.
[21]J. Bialek, A. H. Boozer, M. E. Mauel, and G. A. Navratil, Phys. Plasmas **8**, 2170 (2001).
[22]R. J. La Haye, A. Bondeson, M. S. Chu, A. M. Garofalo, Y. Q. Liu, G. A. Navratil, M. Okabayashi, H. Reimerdes, and E. J. Strait, Nucl. Fusion **44**, 1197 (2004).
[23]Y. Q. Liu, A. Bondeson, C. M. Fransson, B. Lennartson, and C. Breitholtz, Phys. Plasmas **7**, 3681 (2000).
[24]A. H. Glasser and M. C. Chance, Bull. Am. Phys. Soc. **42**, 1848 (1997).
[25]D. P. Brennan, E. J. Strait, A. D. Turnbull *et al.*, Phys. Plasmas **9**, 2998 (2002).
[26]D. Gregoratto, A. Bondeson, M. S. Chu, and A. M. Garofalo, Plasma Phys. Controlled Fusion **43**, 1425 (2001).
[27]H. Reimerdes, J. M. Bialek, M. S. Chance *et al.*, Nucl. Fusion **45**, 368 (2005).
[28]M. von Hellermann, P. Berger, J. Frieling, R. König, W. Mandl, A. Maas, and H. P. Summers, Plasma Phys. Controlled Fusion **37**, 71 (1995).
[29]H. Reimerdes, J. M. Bialek, M. Bigi *et al.*, in *32nd EPS Conference on Plasma Physics and Controlled Fusion*, Tarragona, Spain, 27 June–1 July 2005, edited by C. Hidalgo and B. Ph. van Milligen (European Physical Society, Mulhouse, 2005), Vol. 29C, p. 5.056.
[30]K. C. Shaing, Phys. Plasmas **10**, 1443 (2003).
[31]V. D. Pustovitov, Plasma Phys. Rep. **30**, 187 (2004).
[32]Y. Q. Liu, A. Bondeson, M. S. Chu *et al.*, Nucl. Fusion **45**, 1131 (2005).